www.sciencemag.org/cgi/content/full/310/5754/1668/DC1

Supporting Online Material for

Rapid Glacial Erosion at 1.8 Ma Revealed by $^4He/^3He$ Thermochronometry

David L. Shuster,* Todd A. Ehlers, Margaret E. Rusmore, Kenneth A. Farley

*To whom correspondences should be addressed at Berkeley Geochronology Center, 2455 Ridge Road, Berkeley, CA 94709, USA. E-mail: dshuster@bgc.org

Published 9 December 2005, *Science* **310**, p1668 (2005)
DOI: 10.1126/science.1118519

This PDF file includes:

SOM Text
Figs. S1 to S5
Tables S1 to S5
References and Notes

Supplementary Information for:
Shuster, D.L., T.A. Ehlers, M.E. Rusmore, and K.A. Farley (2005)
Rapid Glacial Erosion at 1.8 Ma Revealed by $^4He/^3He$ Thermochronometry, *Science*

Thermochronometry often involves the determination of a cooling age from parent and daughter abundances within an entire crystal or population of crystals (*1*). Complementary information exists in the spatial concentration distribution of the daughter within a single crystal. By combining a bulk cooling age with the spatial distribution of the daughter on the same sample, it is possible to place tight limits on the sample's time-temperature *(t-T)* path

This approach is applied to the (U-Th)/He system by introducing synthetic ^3He via proton irradiation (*2*). The attraction of the (U-Th)/He system is its sensitivity to uniquely low temperatures. For example, the nominal ^4He closure temperature (at 10^oC/Myr) for apatite is 60^oC (*3*). Therefore, significant diffusion of ^4He occurs at temperatures just slightly higher than those of Earth's surface.

In *$^4He/^3He$ thermochronometry* (*4*), the natural spatial distribution of ^4He is constrained by stepwise degassing $^4He/^3He$ analysis of a sample containing synthetic, proton-induced ^3He. Since the distribution of the ^3He is spatially uniform (*2*), release fractions of proton-induced ^3He can be used to determine the helium diffusion kinetics (*5*) (e.g., Fig. S1-S4, panels (a)). Upon stepwise degassing, sequentially measured $^4He/^3He$ ratios constrain the natural ^4He distribution within an individual crystal or a small population of crystals. Evolution of the $^4He/^3He$ ratio reveals the distribution of radiogenic ^4He within a sample. For instance, a ^4He distribution solely resulting from α-ejection (*6*) (i.e., due to rapid cooling), will have relatively high $^4He/^3He$ ratios at the beginning of a degassing experiment. Conversely, a diffusive ^4He distribution resulting from gradual cooling will have low ^4He near the grain's edge and therefore low initial $^4He/^3He$ ratios which steadily rise over the course of an analysis (*4*). The $^4He/^3He$ ratios of the first ~40% of helium extracted over the course of an analysis contain the highest resolving power on the ^4He distribution (*4*). Note that the $^4He/^3He$ ratios measured toward the end of an experiment are often not useful for constraining the spatial distribution of ^4He in the sample, but must be incorporated when calculating the bulk $^4He/^3He$ ratio of a sample (*7*).

Together, the helium diffusion kinetics and the spatial distribution of ^4He can be used to constrain the sample's *t-T* path. To quantify a sample's thermal history from an observed radiometric age and an inferred spatial distribution of the daughter product is formally an ill posed problem: a set of *t-T* solutions can be constrained, although a single solution does not generally exist. The age and concentration profile together limit acceptable cooling paths.

As discussed in the main text, the $^4He/^3He$ results of 01MR-59 demand rapid cooling of at least 50^oC at between 1.8 Ma and 1.4 Ma. A cooling event of this magnitude should be recorded in proximate samples. Here, we use the $^4He/^3He$ results for samples (TEKI-38, TEKI-34, TEKI-30, and TEKI-23) collected along a nearly vertical profile to test this cooling model. The models presented below are an internally consistent set of solutions that have been bootstrapped from the 01MR-59 result. All models were constrained to a vertical geothermal gradient $\leq 30^oC$/km. From this analysis, we find that all samples at elevation ≤ 2000 m support the occurrence of a rapid cooling event at 1.8 ± 0.2 Ma. Together, the set of solutions places tight constraints on the thermal history of the valley.

Tables S1-S5 ^{4}He/^{3}He thermochronometry data tables for TEKI-38 (**S1**), TEKI-34 (**S2**), TEKI-30 (**S3**) and TEKI-23 (**S4**), and 01MR-59 (**S5**), respectively.

Figures S1-S5 ^{4}He/^{3}He thermochronometry for apatite samples TEKI-38 (**S1**), TEKI-34 (**S2**), TEKI-30 (**S3**), TEKI-23 (**S4**) and 01MR-59 (**S5**), respectively. **(a)** Arrhenius plots; circles are the diffusion coefficients, *D*, normalized to the diffusive length scale, *a*, calculated (*5*) from release fractions of proton-induced ^{3}He (*2*). Solid black line is the inferred helium diffusion kinetics for each sample used to construct models shown in (b,c), determined by linear regression of a subset array. Steps deviate from linearity above 300 °C due to a change in mechanism (*3*) which may not apply to lower temperatures relevant to our models and are therefore excluded from the regression. **(b)** Model *t-T* paths. Each of these models corresponds to the observed (U-Th)/He age for each sample, which is indicated in the lower panels. **(c)** Ratio evolution diagrams. Shown are measured isotope ratios for each release step, R_{step} (R=^{4}He/^{3}He), normalized to the bulk ratio R_{bulk}, plotted versus the cumulative ^{3}He release fraction, ΣF^3He. Each model shown in (c) corresponds to the *t-T* path in (b). Also shown for reference are two end-member ^{4}He distributions, i.e., the α-ejection only distribution (dashed line) and the steady-state distribution (dotted line) (*4*). Due to a change in diffusive mechanism at temperatures >300 °C which were used toward the end of these experiments (*3*), and because the initially extracted gas contains the highest resolving power on the spatial distribution of ^{4}He (*4*), models were matched only to values of ΣF^3He ≤ 0.4. For these reasons, data collected for $\Sigma F^3He > 0.6$ do not well represent the spatial distribution of ^{4}He (*7*) and were not considered in our modeling, although all points were used to calculate the bulk ^{4}He/^{3}He ratio of each sample. Error bars are specified by a vertical line through each point. Data scatter and uncertainty is largely a function of the absolute ^{4}He abundance in each sample and the corresponding magnitude of ^{4}He blank corrections. For instance, TEKI-38 contains a ^{4}He abundance that is 7% of that of TEKI-23.

References

1. M. H. Dodson, *Contributions to Mineralogy and Petrology* **40**, 259 (1973).
2. D. L. Shuster, K. A. Farley, J. M. Sisterson, D. S. Burnett, *Earth and Planetary Science Letters* **217**, 19 (2004).
3. K. A. Farley, *Journal of Geophysical Research* **105**, 2903 (2000).
4. D. L. Shuster, K. A. Farley, *Earth and Planetary Science Letters* **217**, 1 (2004).
5. H. Fechtig, S. Kalbitzer, in *Potassium-Argon Dating* O. A. Schaeffer, J. Zahringer, Eds. (Springer, Heidelberg, 1966) pp. 68-106.
6. K. A. Farley, R. A. Wolf, L. T. Silver, *Geochimica et Cosmochimica Acta* **60**, 4223 (1996).
7. D. L. Shuster, K. A. Farley, in *Low-Temperature Thermochronology: Techniques, Interpretations and Applications* P. W. Reiners, T. A. Ehlers, Eds. (2005), vol. 58, pp. 181-203.

Table S1: TEKI-38

Step	T (oC)	time (hr)	^{3}He (atoms/10^6)	R_{step}/R_{bulk}*	(+/-)
1	150	0.50	0.09	b.d.	b.d.
2	150	0.75	0.06	b.d.	b.d.
3	150	1.00	0.05	b.d.	b.d.
4	175	0.75	0.16	b.d.	b.d.
5	175	1.25	0.18	b.d.	b.d.
6	200	0.75	0.40	b.d.	b.d.
7	200	1.25	0.46	b.d.	b.d.
8	225	0.50	0.60	0.29	0.47
9	225	1.25	1.09	0.42	0.27
10	250	0.75	1.74	0.27	0.17
11	250	1.25	1.81	0.58	0.16
12	240	1.25	0.97	0.53	0.30
13	230	1.50	0.58	b.d.	b.d.
14	220	2.00	0.35	b.d.	b.d.
15	235	2.50	0.89	b.d.	b.d.
16	275	0.75	2.48	0.38	0.12
17	275	1.25	2.55	0.59	0.12
18	300	0.75	3.91	0.50	0.08
19	300	1.25	4.63	0.68	0.07
20	325	0.50	4.57	0.55	0.07
21	325	1.25	8.44	0.69	0.05
22	350	1.25	13.15	0.87	0.03
23	375	0.50	10.37	0.81	0.04
24	425	0.50	22.84	1.03	0.02
25	475	0.50	29.55	1.15	0.02
26	525	0.50	21.76	1.26	0.03
27	575	0.50	5.81	1.51	0.06
28	600	0.50	1.37	1.92	0.22
29	600	1.00	0.49	3.68	0.59
30	600	2.00	0.15	9.66	1.94
31	1200	0.10	0.86	1.73	0.27
Total			142.36		

*R = ^{4}He/^{3}He, R_{bulk} = 26

b.d. is below detection limit

Table S2: TEKI-34

Step	T (oC)	time (hr)	^3He (atoms/10^6)	R_{step}/R_{bulk}*	(+/-)
1	150	0.50	0.12	b.d	b.d
2	150	0.75	0.08	b.d	b.d
3	150	1.00	0.07	b.d	b.d
4	175	0.75	0.24	b.d	b.d
5	175	1.25	0.27	0.37	0.80
6	200	0.75	0.64	0.10	0.34
7	200	1.25	0.72	0.25	0.30
8	225	0.50	0.83	0.26	0.27
9	225	1.25	1.61	0.47	0.14
10	250	0.75	3.32	0.36	0.07
11	250	1.25	3.74	0.52	0.07
12	240	1.25	1.90	0.49	0.12
13	230	1.50	0.88	0.46	0.25
14	220	2.00	0.61	0.46	0.37
15	235	2.50	1.72	0.49	0.14
16	275	0.75	6.03	0.57	0.05
17	275	1.25	6.18	0.63	0.05
18	300	0.75	9.10	0.67	0.03
19	300	1.25	6.32	0.73	0.04
20	325	0.50	5.70	0.69	0.05
21	325	1.25	10.56	0.79	0.03
22	350	1.25	18.14	0.86	0.02
23	375	0.50	12.58	0.97	0.03
24	425	0.50	36.59	1.01	0.02
25	475	0.50	57.06	1.10	0.01
26	525	0.50	53.67	1.21	0.01
27	575	0.50	21.78	1.23	0.02
28	600	0.50	3.31	1.65	0.07
29	600	1.00	1.29	2.14	0.17
30	600	2.00	1.13	2.44	0.19
31	1200	0.10	2.99	0.45	0.09
Total			269.21		

*R = $^4He/^3He$, R_{bulk} = 52

b.d. is below detection limit

Table S3: TEKI-30

Step	T (oC)	time (hr)	^3He (atoms/10^6)	R_{step}/R_{bulk}*	(+/-)
1	150	0.50	0.08	b.d.	b.d.
2	150	0.75	0.04	b.d.	b.d.
3	150	1.00	0.06	b.d.	b.d.
4	175	0.75	0.14	b.d.	b.d.
5	175	1.25	0.15	b.d.	b.d.
6	200	0.75	0.35	0.18	0.64
7	200	1.25	0.36	0.22	0.63
8	225	0.50	0.50	0.19	0.46
9	225	1.25	0.84	0.34	0.29
10	250	0.75	1.53	0.38	0.17
11	250	1.25	1.63	0.43	0.16
12	240	1.25	0.67	0.38	0.36
13	230	1.50	0.47	0.42	0.50
14	220	2.00	0.32	0.26	0.73
15	235	2.50	0.76	0.58	0.32
16	275	0.75	1.65	0.45	0.15
17	275	1.25	2.31	0.61	0.11
18	300	0.75	3.31	0.64	0.08
19	300	1.25	4.29	0.71	0.06
20	325	0.50	3.59	0.71	0.07
21	325	1.25	6.87	0.86	0.04
22	350	1.25	11.87	0.91	0.03
23	375	0.50	7.95	0.93	0.04
24	425	0.50	22.34	1.06	0.02
25	475	0.50	30.99	1.19	0.02
26	525	0.50	26.62	1.15	0.02
27	575	0.50	8.58	1.13	0.04
28	600	0.50	1.16	1.36	0.22
29	600	1.00	0.77	1.45	0.32
30	600	2.00	0.55	2.16	0.45
31	1200	0.10	1.63	1.21	0.06
Total			142.38		

*R = $^4He/^3He$, R_{bulk} = 96

b.d. is below detection limit

Table S4: TEKI-23

Step	T (oC)	time (hr)	^{3}He (atoms/10^{6})	R_{step}/R_{bulk}*	(+/-)
1	150	0.50	0.10	b.d.	b.d.
2	150	0.75	0.10	b.d.	b.d.
3	150	1.00	0.19	b.d.	b.d.
4	175	0.75	0.38	b.d.	b.d.
5	175	1.25	0.39	b.d.	b.d.
6	200	0.75	0.83	b.d.	b.d.
7	200	1.25	0.88	0.35	0.16
8	225	0.50	1.26	0.34	0.12
9	225	1.25	2.15	0.38	0.07
10	250	0.75	2.92	0.45	0.05
11	250	1.25	3.61	0.49	0.04
12	240	1.25	1.65	0.54	0.09
13	230	1.50	1.05	0.55	0.15
14	220	2.00	0.81	0.51	0.19
15	235	2.50	1.95	0.59	0.08
16	275	0.75	3.48	0.56	0.05
17	275	1.25	4.45	0.61	0.04
18	300	0.75	6.70	0.64	0.03
19	300	1.25	7.47	0.71	0.03
20	325	0.50	5.97	0.75	0.03
21	325	1.25	11.01	0.78	0.02
22	350	1.25	18.16	0.89	0.02
23	375	0.50	10.38	0.96	0.02
24	425	0.50	28.16	1.02	0.01
25	475	0.50	36.15	1.12	0.01
26	525	0.50	28.21	1.17	0.01
27	575	0.50	17.64	1.14	0.01
28	600	0.50	9.52	1.13	0.02
29	600	1.00	7.68	1.13	0.03
30	600	2.00	5.24	1.36	0.02
31	1200	0.10	6.56	1.35	0.02
Total			225.04		

*R = $^{4}He/^{3}He$, R_{bulk} = 356

b.d. is below detection limit

Table S5: Apatite 01mr-59

Step	T (oC)	time (hr)	^{3}He (atoms/10^{6})	R_{step}/R_{bulk}*	(+/-)
1	175	0.75	0.35	0.134	0.051
2	175	1.00	0.17	0.183	0.076
3	175	3.00	0.21	0.345	0.127
4	188	1.00	0.13	0.458	0.165
5	188	1.50	0.17	0.423	0.147
6	188	2.00	0.16	0.268	0.108
7	200	0.50	0.08	0.275	0.118
8	200	1.00	0.16	0.368	0.134
9	200	1.50	0.22	0.379	0.126
10	200	2.00	0.27	0.563	0.153
11	225	0.50	0.32	0.663	0.135
12	225	2.00	0.80	0.537	0.080
13	225	2.00	0.73	0.551	0.086
14	250	0.50	0.69	0.724	0.082
15	250	1.00	1.09	0.562	0.057
16	250	2.00	1.51	0.580	0.050
17	275	0.50	1.22	0.615	0.050
18	275	1.00	1.97	0.671	0.036
19	275	2.00	2.87	0.682	0.029
20	295	0.50	1.53	0.691	0.042
21	295	1.00	2.52	0.732	0.029
22	295	2.00	3.80	1.003	0.023
23	305	0.50	1.15	0.819	0.054
24	305	1.00	2.23	0.802	0.032
25	305	1.25	2.30	0.805	0.033
26	305	2.00	3.00	0.834	0.028
27	315	0.50	1.04	0.877	0.060
28	315	1.00	1.91	0.874	0.038
29	315	1.25	1.89	0.912	0.039
30	315	1.75	2.56	0.908	0.032
31	325	0.50	1.01	0.928	0.062
32	325	1.50	2.15	0.981	0.036
33	325	1.50	2.14	0.947	0.036
34	325	2.00	2.30	0.970	0.036
35	335	0.50	0.87	0.971	0.071
36	335	1.00	1.57	0.979	0.066
37	335	1.50	2.00	1.044	0.073
38	335	2.00	2.41	1.121	0.078
39	345	1.00	1.69	1.048	0.082
40	350	0.50	1.00	1.003	0.094
41	360	0.50	1.39	0.973	0.071
42	360	1.00	2.16	1.044	0.034
43	370	0.50	1.58	1.000	0.042
44	370	1.00	2.46	1.026	0.030
45	380	0.50	1.43	1.052	0.046
46	390	0.50	1.73	1.067	0.039
47	400	1.00	3.14	1.307	0.076
48	425	0.50	2.80	1.127	0.025
49	450	0.25	2.07	1.185	0.032
50	450	0.25	1.94	1.111	0.034
51	475	0.25	2.37	1.120	0.028
52	475	0.25	1.46	1.151	0.044
53	475	0.50	1.61	1.362	0.042
54	475	0.50	0.89	1.445	0.073
55	500	0.25	0.62	1.467	0.097
56	500	0.25	0.34	1.593	0.162
57	550	0.50	0.71	1.693	0.156
58	550	0.75	0.45	2.602	0.363
59	550	1.00	0.43	1.895	0.339
60	550	3.00	0.47	1.538	0.317
61	525	5.00	0.72	1.619	0.260
62	525	5.00	0.62	1.330	0.268
63	600	5.00	0.97	1.535	0.208
64	600	5.00	0.88	1.615	0.228
65	620	5.00	0.72	1.663	0.263
66	1200	0.10	1.74	1.660	0.271
Total			89.89		

*R = ^{4}He/^{3}He, R_{bulk} = 236

Shuster, Ehlers, Rusmore, Farley (2005)
Figure S1

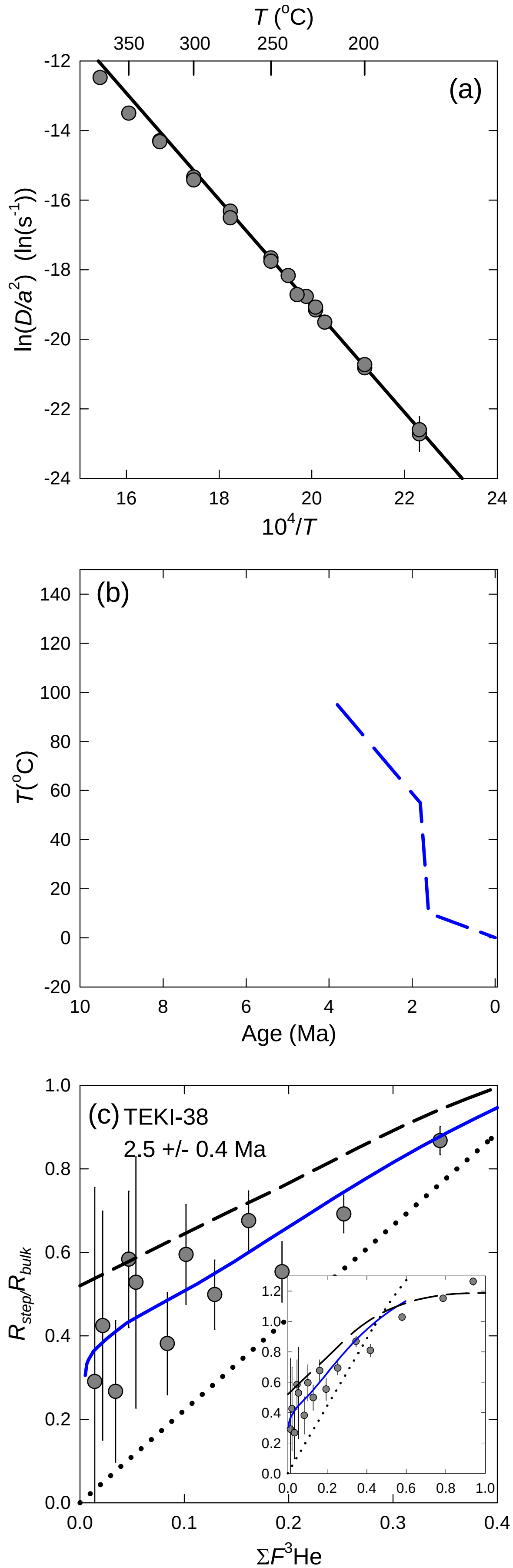

Shuster, Ehlers, Rusmore, Farley (2005)
Figure S2

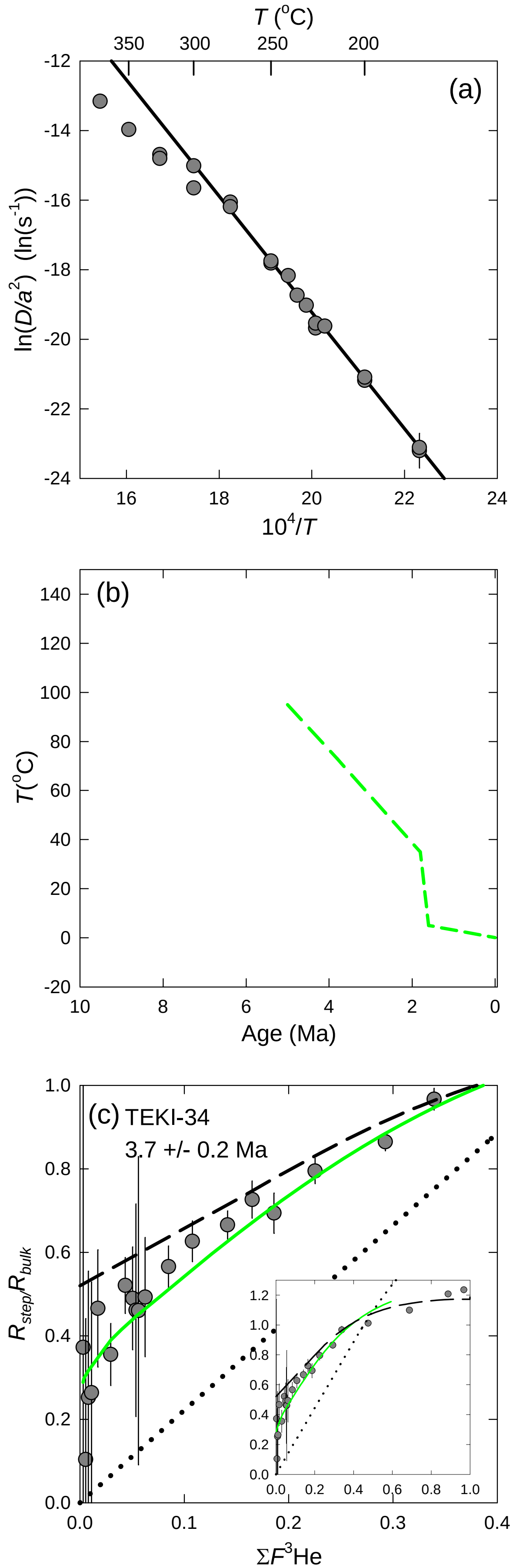

Shuster, Ehlers, Rusmore, Farley (2005)
Figure S3

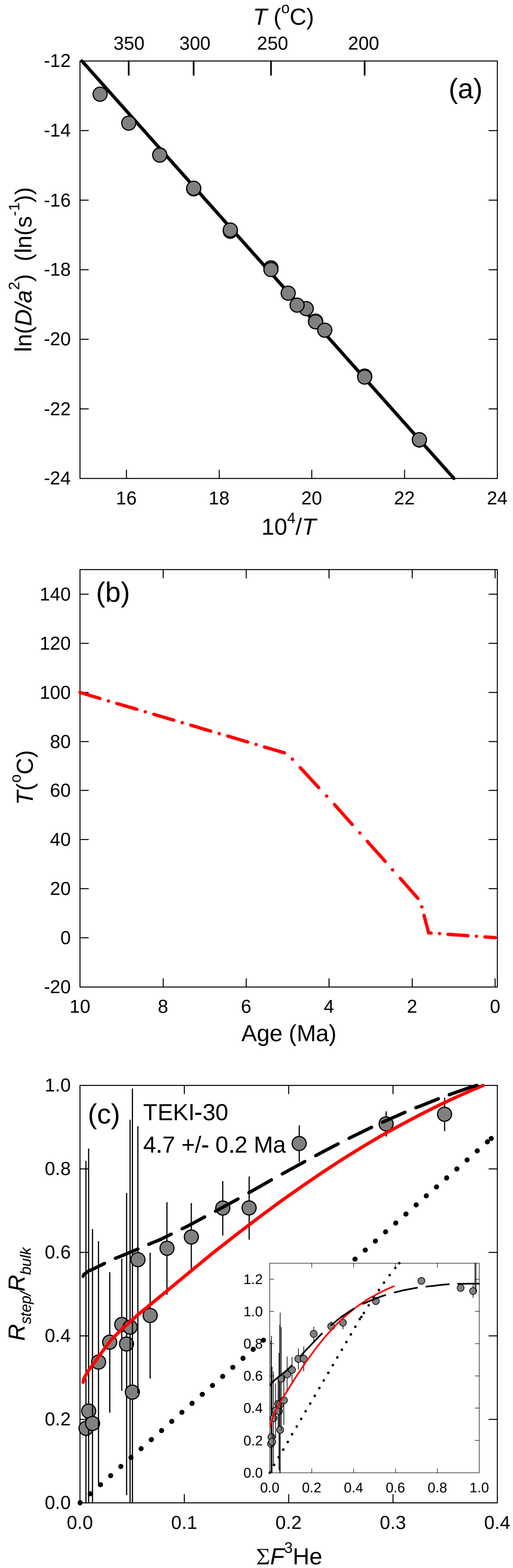

TEKI-30

4.7 +/- 0.2 Ma

Shuster, Ehlers, Rusmore, Farley (2005)
Figure S4

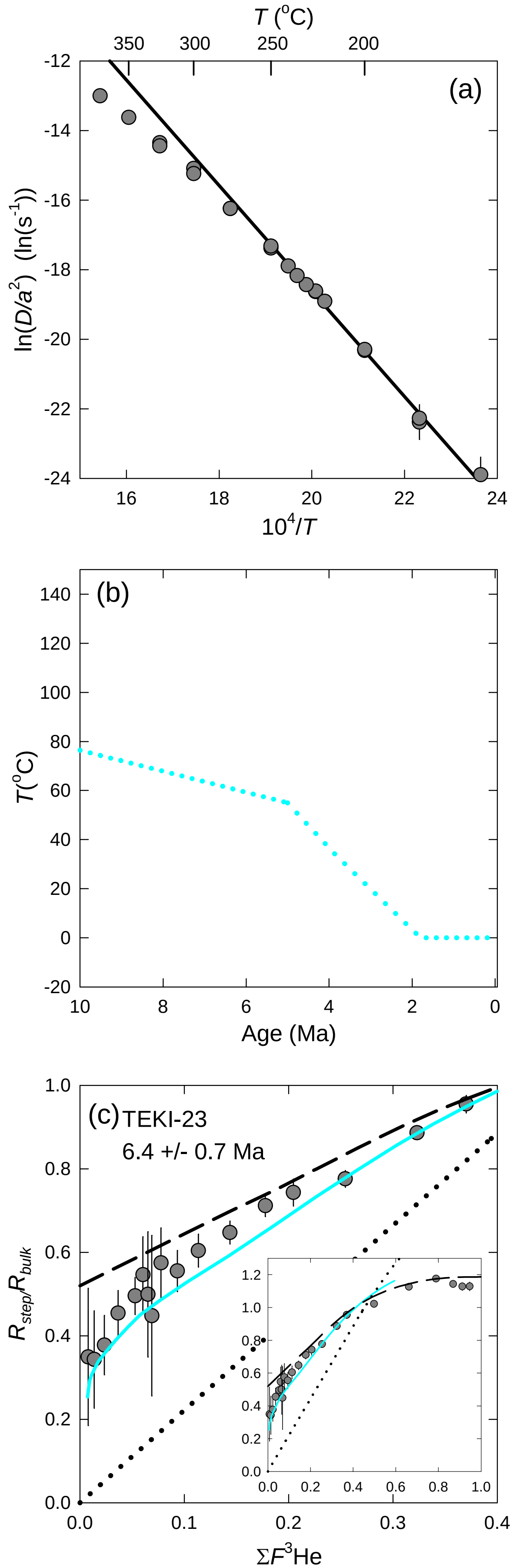

Shuster, Ehlers, Rusmore, Farley (2005)
Figure S5